

Lawrence Berkeley National Laboratory

Recent Work

Title

Spectroscopic Characterization of Aqua [fac-Tc(CO)₃]⁺ Complexes at High Ionic Strength.

Permalink

<https://escholarship.org/uc/item/20d52585>

Journal

Inorganic chemistry, 57(12)

ISSN

0020-1669

Authors

Chatterjee, Sayandev
Hall, Gabriel B
Engelhard, Mark H
et al.

Publication Date

2018-06-01

DOI

10.1021/acs.inorgchem.8b00490

Peer reviewed

Spectroscopic Characterization of Aqua $[fac\text{-Tc}(\text{CO})_3]^+$ Complexes at High Ionic Strength

Sayandev Chatterjee,[†] Gabriel B. Hall,[†] Mark H. Engelhard,[‡] Yingge Du,[‡] Nancy M. Washton,[‡] Wayne W. Lukens,[&] Tatiana G. Levitskaia^{*†}

[†]Energy and Environment Directorate, Pacific Northwest National Laboratory, Richland, Washington 99354, United States; email: Tatiana.Levitskaia@pnnl.gov

[‡]Environmental Molecular Sciences Laboratory, Pacific Northwest National Laboratory, Richland, Washington 99354, United States

[&] Lawrence Berkeley National Laboratory, Berkeley, California 94720, United States

Abstract

Despite the importance of fundamental understanding of Tc properties and behavior to both the remediation of nuclear waste and the reprocessing of nuclear fuel, the current knowledge of the electronic structure, and spectral signatures of low-valent Tc compounds significantly lags behind the remainder of the *d*-block elements. In particular, identification and treatment of Tc compounds in legacy nuclear waste is challenging due to the lack of reference data. A spectroscopic library corresponding to the relevant conditions of extremely high ionic strength needs to be established in the scientific literature for Tc compounds, particularly in the less common oxidation states. To this end, $[fac\text{-Tc}(\text{CO})_3\text{Cl}_3]^{2-}$ and compounds with the general formula of $[fac\text{-Tc}(\text{CO})_3(\text{OH}_2)_{3-n}(\text{OH})_n]^{1-n}$ are examined by ⁹⁹Tc NMR, ¹³CO NMR, IR, XPS, and XAS spectroscopies. This includes the first observations of these compounds by XAS and $[fac\text{-Tc}(\text{CO})_3\text{Cl}_3]^{2-}$ by XAS. The independent spectroscopic techniques all show a consistent trend of an increasing metal center electron density as H₂O ligands are replaced by ⁻OH. The lone exception is $[fac\text{-Tc}(\text{CO})_3(\text{OH})]_4$ which exhibits a comparatively low electron density at the metal center. This is attributed to the μ -bridging nature of the ⁻OH ligands causing them to be weaker σ -donors.

Introduction

Since the discovery of tricarbonyl complexes of the group 7 transition elements (Mn, Tc, and Re) in the 1950's,¹ their fundamental organometallic chemistry has received attention due to the kinetic inertness and thermodynamic stability of the low-spin, $d^6\text{-}[fac\text{-M}(\text{CO})_3]^+$ configuration.²⁻⁴ The increasing applicability of group 7 tricarbonyl complexes in the fields of catalysis, green chemistry, and drug design has motivated significant expansion of the knowledge base related to their aqueous chemistry. While comprehensive studies have been performed on the Mn and Re systems, allowing a deep understanding of the effect of ancillary ligands on the electronic structure and reactivity of the $[fac\text{-M}(\text{CO})_3]^+$ framework, studies on the analogous $[fac\text{-Tc}(\text{CO})_3]^+$ complexes remain far fewer. Of particular significance are the

aqua $[fac\text{-Tc}(\text{CO})_3(\text{OH}_2)_3]^+$ complex and its congeners because of their importance in the field of nuclear medicine and nuclear waste processing.

In the field of nuclear energy, improved operation of modern nuclear reactors and increasing demand for non-CO₂-emitting power facilitates expansion of nuclear power production, which is driving research into improved irradiated fuel partitioning and waste management strategies. Technetium-99 (Tc) is a high yield byproduct of the thermal neutron fission of ²³⁵U and ²³⁹Pu generated in significant quantities in nuclear reactors, and its inventory continually increases due to nuclear power generation world-wide.⁵ Technetium is a major risk-driver during processing and storage of used nuclear fuel and legacy nuclear waste generated during the Cold War era, which is currently stored in multiple locations world-wide such as United States Department of Energy (DOE) Hanford site.⁶ Among radioactive constituents in the Hanford tank waste, ⁹⁹Tc presents a unique challenge. The long half-life ($\beta = 292$ keV; $t_{1/2} = 2.11 \times 10^5$ y), complex chemical behavior, and high mobility in subsurface environments make Tc one of the most challenging radionuclides to dispose of and/or remediate. These issues also create significant dose implications in performance assessments of Tc long-term storage and disposition sites that rely on high durability waste forms. Successful separation and treatment of Tc during tank waste processing is a critical technical challenge for the nuclear waste management. Technetium can adopt a wide range of oxidation states (from -I to +VII) and will be present in multiple chemical forms depending on solution conditions. Understanding Tc speciation is a key to developing tank waste management strategies, nuclear fuel cycle separations, and remediation of the contaminated subsurface plumes.

The current knowledge of Tc redox and thermodynamic behavior presumes that the highly alkaline, high ionic strength matrices in tank waste supernatants will be dominated by the Tc(VII) oxidation state. However, this assumption was contradicted by two observations. First, previous attempts to separate Tc from the liquid fraction of the tank waste using an ion-exchange processes specific to pertechnetate (TcO_4^-) met with limited success particularly for the wastes with high organic content.⁷⁻⁹ This implies that a significant fraction of the soluble Tc is present as low-valent Tc (oxidation state $< +7$) due to the reductive conditions generated by the radiolysis products of water, nitrate, and other constituents and stabilized by the organic complexants present in the waste. Second, the presence of the low-valent Tc species has been confirmed by the direct Tc K-edge X-ray absorbance spectroscopic measurements of the Hanford tank waste samples; the obtained spectra could be reasonably fit to the spectrum of the gluconate or hydroxide-coordinated $[fac\text{-Tc}(\text{CO})_3]^+$ complex leading to their tentative identification as $[fac\text{-Tc}(\text{CO})_3]^+$ (or possibly $[fac\text{-Tc}(\text{CO})_2(\text{NO})]^{2+}$) derivatives.¹⁰ This discovery is surprising considering the highly alkaline brine-like nature of the Hanford tank waste and could be potentially attributed to the formation of kinetically inert complexes with a variety of mono-, bis-, and tridentate ligand systems, some of which, including nitrilotriacetate, ethylenediaminetetraacetate, citrate, and gluconate, have been found in the tank waste. Identification and thorough understanding of the molecular structure of these $[fac\text{-Tc}(\text{CO})_3]^+$ species in the actual tank waste is useful for designing effective Tc separation and immobilization strategies. Such identification largely relies on the direct spectroscopic characterization of the tank waste samples as any manipulations leading to the changes in matrix compositions would likely result in the redox and/or chemical alteration of the original composition.¹¹ One complicating factor is extensive hydrolysis of the parent $[fac\text{-Tc}(\text{CO})_3(\text{OH}_2)_3]^+$ species at alkaline pH, resulting hydrolysis products of general composition $[fac\text{-Tc}(\text{CO})_3(\text{OH}_2)_{3-n}(\text{OH})_n]^{1-n}$ ($n = 0-3$) may interfere with complexation of inorganic and organic ligands in the alkaline tank environment and potentially form mixed ligand hydroxo complexes. Therefore, availability of the reliable spectroscopic database of the relevant compounds is imperative for the identification of the $[fac\text{-Tc}(\text{CO})_3]^+$ species in the actual tank waste.

Properties of the $[fac\text{-Tc}(\text{CO})_3(\text{OH}_2)_3]^+$ species and their first hydrolysis product have been extensively investigated in the simple aqueous systems from mildly acidic to alkaline solutions due to their relevance to the nuclear medicine application.¹² The second hydrolysis product has been reported only rarely¹⁰ because it is only formed in highly alkaline solutions and hence is not of interest to the development of radiopharmaceuticals. Gorshkov and coworkers¹³ studied the various $[fac\text{-Tc}(\text{CO})_3]^+$ hydrolysis products of the formula $[fac\text{-Tc}(\text{CO})_3(\text{OH}_2)_{3-n}(\text{OH})_n]^{1-n}$ by ⁹⁹Tc nuclear magnetic resonance spectroscopy. Alberto and coworkers reported the infra-red spectroscopic data on select $[fac\text{-Tc}(\text{CO})_3]^+$ species.¹⁴ Significant progress has been achieved in understanding of the ligand exchange kinetics and coordination of $[fac\text{-Tc}(\text{CO})_3(\text{OH}_2)_3]^+$ using multi-nuclear NMR studies as evident from a recent review.¹⁵ However, none of these studies were conducted in high ionic strength matrices characteristic of tank waste supernatants. Furthermore, there is no systematic knowledge regarding electronic properties of the aqua $[fac\text{-Tc}(\text{CO})_3]^+$ complexes, and to date NMR remains nearly a sole technique applied for their characterization. Notably, X-ray photoelectron spectroscopy (XPS) can yield direct information on how the nature of an ancillary ligand coordinated to the $[fac\text{-Tc}(\text{CO})_3]^+$ moiety affects the electronic properties of the Tc(I) center, however such data are lacking. To date, only few XPS studies of Tc (0-VII) compounds have been reported.^{16,17}

This work focuses on the systematic characterization of non-chelated aqua $[fac\text{-Tc}(\text{CO})_3]^+$ species under high ionic strength conditions typical for the legacy tank waste by NMR, infrared, XPS and X-ray Absorption spectroscopy. This is our initial effort to develop a spectroscopic library for the complexes of the form $[fac\text{-Tc}(\text{CO})_3(\text{OH}_2)_{3-n}(\text{OH})_n]^{1-n}$ ($n = 0\text{-}3$), while providing insight into the effect of varying ancillary ligand on the electronic structure of the $[fac\text{-Tc}(\text{CO})_3]^+$ framework. To expand our understanding of the observed trends, we included $[fac\text{-Tc}(\text{CO})_3\text{Cl}_3]^{2-}$ complex in the array of the studied compounds. This will allow us to evaluate likelihood of their presence in the tank waste by characterizing the spectral fingerprints of individual species and their reactivity toward organic chelators.

Materials

Radiation safety disclaimer! Technetium-99 has a half-life of 2.12×10^5 years and emits a low-energy (0.292 MeV) β particle; common laboratory materials provide adequate shielding. Radiation safety procedures must be used at all times to prevent contamination.

In-house NH_4TcO_4 stock, available at the Radiochemical Processing Laboratory (RPL) at Pacific Northwest National Laboratory (PNNL), was used. Acetonitrile, diethyl ether, dichloromethane, and borane-tetrahydrofuran (BH_3/THF) complex were obtained from Sigma-Aldrich and used without further purification. Gaseous CO used in the synthesis of the $(\text{Et}_4\text{N})_2[\text{Tc}(\text{CO})_3\text{Cl}_3]$ was obtained from Matheson Tri-Gas, while the ¹³C labeled analog ¹³CO was obtained from Cambridge Isotope Library. Argon gas also was obtained from Matheson. All inorganic sodium salts (including nitrate and hydroxide) were obtained from Sigma-Aldrich and were of reagent grade. All aqueous solutions were prepared from water deionized to $\geq 15\text{ M}\Omega$ with a Barnstead Nanopure water purification system.

Synthesis of $[fac\text{-Tc}(\text{CO})_3]^+$ compounds

$[\text{Et}_4\text{N}]_2[\text{fac}\text{-Tc}(\text{CO})_3\text{Cl}_3]$ was prepared by a two-step reduction procedure, which involved (a) an initial reduction of ammonium pertechnetate to a Tc(V) isolated as $(\text{Bu}_4\text{N})[\text{TcOCl}_4]$ solid and (b) its subsequent reduction in presence of CO to Tc(I) in the form of $[fac\text{-Tc}(\text{CO})_3\text{Cl}_3]^{2-}$ which was isolated as

the $(\text{Et}_4\text{N})_2[\text{fac-Tc}(\text{CO})_3\text{Cl}_3]$ product by precipitation.¹⁸ It was used to generate analytically pure tetrameric $[\text{Tc}(\text{CO})_3(\text{OH})]_4$ species according to modified literature procedure¹⁹ by dissolution in aqueous 0.1 M NaOH solution and extraction of the product into diethyl ether. The preparation of the ^{13}C analogs involved similar preparation of $[\text{Et}_4\text{N}]_2[\text{fac-Tc}(^{13}\text{CO})_3\text{Cl}_3]$ and $[\text{fac-Tc}(^{13}\text{CO})_3(\text{OH})]_4$ complexes using gaseous ^{13}CO . These two complexes, $[\text{Et}_4\text{N}]_2[\text{fac-Tc}(\text{CO})_3\text{Cl}_3]$ and $[\text{Tc}(\text{CO})_3(\text{OH})]_4$ were used to generate aqueous $[\text{fac-Tc}(\text{CO})_3]^+$ species of the general formulae $[\text{fac-Tc}(\text{CO})_3(\text{OH}_2)_{3-n}(\text{OH})_n]^{1-n}$ ($n=0-3$). These species were obtained by dissolving the $[\text{fac-Tc}(\text{CO})_3\text{Cl}_3]^{2-}$ or the $[\text{fac-Tc}(\text{CO})_3(\text{OH})]_4$ precursors in 5 M NaNO_3 / 0.1 M HNO_3 to obtain $[\text{fac-Tc}(\text{CO})_3(\text{OH}_2)_3]^+$ or in 5 M NaNO_3 / 0.1 M NaOH and 5 M NaNO_3 / 6.2 M NaOH to obtain $[\text{fac-Tc}(\text{CO})_3(\text{OH}_2)_2(\text{OH})]$ and $[\text{fac-Tc}(\text{CO})_3(\text{OH}_2)(\text{OH})_2]^{1-}$, respectively. For each product, ^{99}Tc NMR spectrum was collected and showed a single $[\text{fac-Tc}(\text{CO})_3]^+$ resonance confirming presence of a single $[\text{fac-Tc}(\text{CO})_3]^+$ species.

Spectroscopic techniques

Technetium-99 nuclear magnetic resonance (NMR) spectroscopy.

Sample solutions were placed in capped polytetrafluoroethylene (PTFE)/fluorinated ethylene propylene (FEP) copolymer sleeves (Wilmad), which were then inserted into 5- or 10-mm glass NMR tubes to provide secondary containment for the radioactive liquid. Technetium-99 NMR data were collected at 67.565 MHz on a 300 MHz Tecmag Discovery spectrometer equipped with a 10-mm broadband Nalorac probe²⁰ or at 168.71339 MHz on a 17.6 T (750 MHz) Bruker Avance III spectrometer equipped with a 5-mm broadband Bruker probe. A calibrated $\pi/4$ pulse of 11.80 μs was utilized after determining this to be the optimal pulse width for exciting the largest bandwidth, as determined by transfer function analysis via Mathematica. 12000 to 96000 transients were acquired with a 400 KHz sweep width centered at -900 ppm, and a 0.50 s recycle delay. Chemical shifts were referenced to internal aqueous pertechnetate (TcO_4^-) at 0 ppm (note that the chemical shift of TcO_4^- (aq) is sensitive to ionic strength, resulting in ^{99}Tc resonances that varied from 3 to 8 ppm prior to setting them to zero). Time domain free induction decays were zero filled once and apodized with exponential functions corresponding to 50 Hz of Lorentzian broadening prior to Fourier transformation. A solution containing 10 mM $[\text{TcO}_4]^-$ was used as a ^{99}Tc chemical shift reference, and all chemical shift data are quoted relative to a small $[\text{TcO}_4]^-$ resonance that is present in all the aqueous solutions due to the inherent tendency of the $[\text{fac-Tc}(\text{CO})_3]^+$ to undergo oxidative decomposition to Tc(VII) with time.²¹

^{13}C direct detect experiments were performed on a 17.6 T (750 MHz) Bruker Avance III spectrometer equipped with a 5-mm broadband HDX Bruker probe operating at a frequency of 188.68448 MHz. 256 to 12288 transients were acquired using calibrated $\pi/2$ pulses of 9.5 μs , a 100 KHz sweep width centered at 200 ppm to optimize detection of the $^{13}\text{C}\equiv\text{O}$ resonance, and a 5.0 s recycle delay. Chemical shifts were referenced to external tetramethylsilane (TMS), although the resonances are slightly shifted due to the salt content of the samples. Time domain free induction decays were zero filled once and apodized with exponential functions corresponding to 50 Hz of Lorentzian broadening prior to Fourier transformation.

FTIR Spectroscopy

FTIR measurements were conducted using an attenuated total reflectance (ATR)-FTIR spectrometer (ALPHA model, Bruker Optics) operated with OPUS software (Version 6.5 Build 6.5.92). Samples were run directly on a diamond ATR cell. For each sample, 24 scans with a resolution of 4 cm^{-1} were averaged to give the final spectrum. A background of ambient air was used for all samples. A sample volume of

approximately 10 μL was used for each analysis; this was adequate to cover the collection region of the ATR cell.

X-ray photoelectron spectroscopy

X-ray photoelectron spectroscopy (XPS). X-ray photoelectron spectra were recorded using a Kratos AXIS Ultra DLD system equipped with a monochromatic Al $K\alpha$ x-ray source (1486.7 eV) and a hemispherical analyzer. Samples were mounted using double-sided Scotch brand tape attached to a silicon substrate. The instrument work function was calibrated to give a binding energy (BE) of 83.96 ± 0.1 eV for the Au $4f_{7/2}$ line for metallic gold and the spectrometer dispersion was adjusted to give a BE of 932.62 ± 0.1 eV for the Cu $2p_{3/2}$ line of metallic copper. High resolution analyses were carried out with an analysis area of 300×700 microns using a pass energy of 40 eV with a step size of 0.1 eV. Surface charge was eliminated with a charge neutralizer, and data were corrected through referencing the 285.0 eV C 1s peak. The percentages of individual elements detected were determined from the relative composition analysis of the peak areas of the bands on the basis of the relative peak areas and their corresponding sensitivity factors to provide relative compositions. XPS peak fitting was performed using CasaXPS.

For the XPS measurements, the solid $[\text{Et}_4\text{N}]_2[\text{fac-Tc}(\text{CO})_3\text{Cl}_3]$ and $[\text{fac-Tc}(\text{CO})_3(\text{OH})]_4$ samples were prepared by the deposition onto a carbon tape. The XPS samples containing various $[\text{fac-Tc}(\text{CO})_3(\text{OH}_2)_3 \cdot n(\text{OH})_n]^{1-n}$ species were prepared by depositing drops of freshly prepared solutions onto the tape and evaporating to a solid under normal atmospheric conditions.

X-ray absorption spectroscopy (XAS)

XAS data were obtained either at SSRL BL 11-2 for $[\text{Et}_4\text{N}]_2[\text{fac-Tc}(\text{CO})_3\text{Cl}_3]$ and $[\text{fac-Tc}(\text{CO})_3(\text{OH})]_4$ and at APS BL-12 BM for the rest of the compounds. X-ray absorption near edge structure spectroscopy (XANES) data were obtained from 200 eV below the Tc edge to 1000 eV above the edge; the data from 75 eV below the edge to 200 eV above the edge was obtained with 0.5 eV spacing. The rest of the data points are widely spaced (50 eV) and were used for the pre- and post-edge correction. The monochromator was detuned 50% to reduce the harmonic content of the beam. Transmission data was obtained using Ar filled ion chambers. Fluorescence data were obtained using a 100 element Ge detector and were corrected for detector dead time. Data were converted from raw data to spectra using SixPack.²² Spectra were normalized using Artemis to process raw data.²³ Normalized XANES spectra were fit using standard spectra in the program "fites," which is part of the RSXAP X-ray spectroscopy analysis suite. XANES standard spectra were carefully energy calibrated using TcO_4^- adsorbed on Reillex-HPQ as the energy reference. The XANES spectra of the "unknown" samples were allowed to vary in energy during fitting. The XANES spectral resolution is 7 eV based on the width of the TcO_4^- pre-edge peak, so each spectrum possesses 14 independent data points (range of the spectrum divided by the resolution). XANES spectra for the samples were convolved with a 1.7 eV Gaussian to match to the energy resolution of the TcO_2 and TcO_4^- reference spectra, and the XANES spectrum of $[\text{fac-Tc}(\text{CO})_3(\text{OH}_2)_2(\text{OH})]$ was convolved with a 1.5 eV Gaussian for the same reason. For $[\text{Et}_4\text{N}]_2[\text{fac-Tc}(\text{CO})_3\text{Cl}_3]$, EXAFS data were fit using theoretical scattering factors calculated for a model $[\text{fac-Tc}(\text{CO})_3\text{Cl}_3]^{2-}$ compound based on the structural parameters and distances obtained from its crystal structure.¹⁴ The value of S_0^2 for this and other fittings was determined to be 1.0 by modeling several EXAFS spectra of TcO_4^- , for which the coordination number is 4.

Results and discussions

^{99}Tc NMR spectroscopy of ^{13}C labeled species

The ^{99}Tc NMR spectra of $[\text{fac-Tc}(^{13}\text{CO})_3(\text{OH})_{3-n}(\text{OH})_n]^{1-n}$ compounds can be viewed in **Error! Reference source not found.**, and the chemical shifts are tabulated in **Error! Reference source not found.** The resonance for the labeled $[\text{fac-Tc}(^{13}\text{CO})_3(\text{OH})]_4$ material shows a quartet resonance at -565.8 ppm in aqueous 5 M NaNO_3 solution, due to $^1J_{^{99}\text{Tc},^{13}\text{C}}$ coupling of each of the four chemically equivalent ^{99}Tc nuclei with three equivalent ^{13}CO . The $^1J_{^{99}\text{Tc},^{13}\text{C}}$ coupling constant is ~1670 Hz.

$[\text{fac-Tc}(^{13}\text{CO})_3(\text{OH})_{3-n}(\text{OH})_n]^{1-n}$ ($n=0-3$) species were independently generated from $[\text{fac-Tc}(^{13}\text{CO})_3(\text{OH})]_4$ through dissolution of the tetramer in aqueous solutions and careful adjustment of solution pH, acidity or alkalinity based on the NMR titration results obtained on the unlabeled species. Therefore, $[\text{fac-Tc}(^{13}\text{CO})_3(\text{OH})_3]^+$ was generated by dissolving $[\text{fac-Tc}(^{13}\text{CO})_3(\text{OH})]_4$ in 5 M NaNO_3 and changing the pH to 1. Raising the pH of the aqueous solution to 12.5 resulted in exclusive formation of $[\text{fac-Tc}(^{13}\text{CO})_3(\text{OH})_2(\text{OH})]^-$. To generate $[\text{fac-Tc}(^{13}\text{CO})_3(\text{OH})_2(\text{OH})_2]^{2-}$, the tetramer was separately dissolved in a 6.2 M NaOH matrix. As shown in Table 1, the trend in ^{99}Tc chemical shifts are $[\text{fac-Tc}(\text{CO})_3(\text{OH})]_4 > [\text{fac-Tc}(\text{CO})_3(\text{OH})_2]_3^+ > [\text{fac-Tc}(\text{CO})_3(\text{OH})_2(\text{OH})] > [\text{fac-Tc}(^{13}\text{CO})_3(\text{OH})_2(\text{OH})_2]^{2-}$, which is roughly correlated with the amount of electron density at the ^{99}Tc center -- $[\text{fac-Tc}(\text{CO})_3(\text{OH})]_4$ is the most electron rich and $[\text{fac-Tc}(\text{CO})_3(\text{OH})]_4$ is the most electron poor. For comparison, the chemical shift of $[\text{fac-Tc}(\text{CO})_3\text{Cl}_3]$ is -1008 ppm, which places it between $[\text{fac-Tc}(\text{CO})_3(\text{OH})_2(\text{OH})]^-$ and $[\text{fac-Tc}(^{13}\text{CO})_3(\text{OH})_2(\text{OH})_2]^{2-}$ in the series.

The ^{99}Tc NMR spectrum of $[\text{fac-Tc}(^{13}\text{CO})_3(\text{OH})_3]^+$ shows a quartet centered at -865 ppm, consistent with ^{99}Tc bonded to three equivalent ^{13}CO .²⁴ For the species of $[\text{fac-Tc}(^{13}\text{CO})_3(\text{OH})_2(\text{OH})]^-$, and $[\text{fac-Tc}(^{13}\text{CO})_3(\text{OH})_2(\text{OH})_2]^{2-}$ the splitting pattern is potentially more complicated. In the event of slow ligand exchange, the expected pattern is a doublet of triplets or conversely a triplet of doublets due to two inequivalent ^{13}CO environments; the two ^{13}CO ligands occupying *trans* positions with respect to the H_2O ligands are chemically inequivalent to the one ^{13}CO ligand occupying a *trans* position with respect to the OH^- group. However, if ligand exchange is rapid, the ^{13}CO environments will be equivalent and the splitting pattern will be a quartet.

The tendency of solvent available ligands (i.e. H_2O and OH^-) to undergo exchange is well-documented^{2,15,24,25}. The exchange of water on $[\text{fac-Tc}(^{13}\text{CO})_3(\text{OH})_3]^+$ has been documented as too slow on the NMR time scale to cause line broadening, and thus equivalent ^{13}CO environments in this case. However, another mechanism for rapid exchange of the positions of the hydroxide and aqua ligands on $[\text{fac-Tc}(^{13}\text{CO})_3(\text{OH})_2(\text{OH})]^-$ and $[\text{fac-Tc}(^{13}\text{CO})_3(\text{OH})_2(\text{OH})_2]^{2-}$ exists. Namely, the O atoms remaining stationary and undergoing rapid protonation or deprotonation will cause a magnetic equivalence of CO ligands on the NMR time scale.

The observed splitting pattern is a sextet, which occurs because of two ^{13}CO environments with overlapping splitting patterns. A similar effect is also anticipated for $[\text{fac-Tc}(^{13}\text{CO})_3(\text{OH})_2(\text{OH})_2]^{2-}$. However, the resolution of the multiplet lines is poorly resolved compared to $[\text{fac-Tc}(^{13}\text{CO})_3(\text{OH})_2(\text{OH})]^-$. Multiple explanations exist for decreased resolution of this peak, including a change in relaxation rate due to the increase in molecular charge or an increase in ion pairing arising from an increase in molecular charge. Unfortunately, the high ionic strength matrices precluded temperature dependent NMR studies due to the possibility of the electrolytes precipitating and altering the ionic strengths. The sextet of the

[*fac*-Tc(¹³CO)₃(OH₂)(OH)₂]⁻ and [*fac*-Tc(¹³CO)₃(OH₂)₂(OH)] spectra show that the rate of proton exchange is slow on the NMR time scale.

The ¹J_{99Tc,13C} coupling constant for [*fac*-Tc(¹³CO)₃(OH₂)₃]⁺ is 355 Hz. For [*fac*-Tc(¹³CO)₃(OH₂)₂(OH)] and [*fac*-Tc(¹³CO)₃(OH₂)(OH)₂]⁻ two coupling constants are expected. However due to similarity in the coupling constant values, they appear as a sextet with a ¹J_{99Tc,13C} value of 345 Hz for the former and 362 Hz for the latter respectively. The appearance of the quartet for [*fac*-Tc(¹³CO)₃(OH₂)₃]⁺ is consistent with that observed by Aebischer *et al.*²⁴

¹³C NMR spectroscopy of ¹³C labeled species

The ¹³CO region of the ¹³C NMR spectrum of [*fac*-Tc(¹³CO)₃(OH)]₄ in 5 M NaNO₃, shows a broad resonance at centered at 211.4 ppm as displayed in **Error! Reference source not found.** However, the resonance splitting is well resolved for the [*fac*-Tc(¹³CO)₃(OH₂)₃]⁺ species, showing a decet centered at 210.7 ppm. The ¹J_{99Tc,13C} coupling constant is observed to be 354 Hz, consistent with that observed in the ⁹⁹Tc NMR spectrum. The resonances become progressively less resolved for [*fac*-Tc(¹³CO)₃(OH₂)₂(OH)] and [*fac*-Tc(¹³CO)₃(OH₂)(OH)₂]⁻. Along the series [*fac*-Tc(¹³CO)₃(OH₂)₃]⁺, [*fac*-Tc(¹³CO)₃(OH₂)₂(OH)] and [*fac*-Tc(¹³CO)₃(OH₂)(OH)₂]⁻, the ¹³C chemical shift for the ¹³CO is observed to progressively move to more positive values (δ(¹³CO): [*fac*-Tc(¹³CO)₃(OH₂)₂(OH)], 213.4 ppm; [*fac*-Tc(¹³CO)₃(OH₂)(OH)₂]⁻, 214.6 ppm).

FTIR spectroscopy of [*fac*-Tc(CO)₃]⁺ complexes

The IR spectrum of the isolated solid (Et₄N)₂[Tc(CO)₃Cl₃] material agrees well with literature showing the presence of the characteristic Tc-C≡O vibration bands at 2017, 1912, and 1889 cm⁻¹, and the fingerprint region exhibiting bands at 1462, 1181, 795, 675, 648, and 485 cm⁻¹. The highest energy carbonyl stretch is attributed to the carbonyl A₁ vibrational mode while the lower two bands are attributed to the splitting of the carbonyl E vibrational mode due to imperfect C_{3v} symmetry.¹⁴ The remaining compounds that were examined, [*fac*-Tc(CO)₃(OH₂)₃]⁺, [*fac*-Tc(CO)₃(OH)]₄, [*fac*-Tc(CO)₃(OH₂)₂(OH)], and [*fac*-Tc(CO)₃(OH₂)(OH)₂]⁻, show a similar splitting pattern but are shifted to either higher or lower frequencies depending on ligand substitution.

The stretching frequencies shift from low energy to high energy in the order [*fac*-Tc(CO)₃(OH₂)(OH)₂]⁻ < [Tc(CO)₃Cl₃]²⁻ < [*fac*-Tc(CO)₃(OH₂)₂(OH)] < [*fac*-Tc(CO)₃(OH)]₄ < [*fac*-Tc(CO)₃(OH₂)₃]⁺ as shown in **Error! Reference source not found.** and **Error! Reference source not found.** The FTIR spectra suggest that the electron density present at the metal center increases in the inverse order of the carbonyl stretching frequency with the greatest Tc electron density present in [Tc(CO)₃(OH₂)(OH)₂]⁻ and the least Tc electron density present in [*fac*-Tc(CO)₃(OH₂)₃]⁺. This ordering is consistent with anionic ⁻OH having a greater σ-donating and π-donating effect than the neutral OH₂; therefore, the electron density at the metal center increases as the number of ⁻OH groups is increased. Greater electron density is manifested in increased π-backbonding of the metal center *d*-orbitals to the π* orbitals of CO, which lowers the CO bond order and consequently the stretching frequency. Cl⁻ is a weaker donor than ⁻OH but stronger than neutral OH₂, which is reflective of the combination of three Cl⁻ in [Tc(CO)₃Cl₃]²⁻ showing similar effect as the combination of two OH₂ and one ⁻OH in [*fac*-Tc(CO)₃(OH₂)₂(OH)]. The tetrameric species, [*fac*-Tc(CO)₃(OH)]₄ shows considerably less Tc electron density than the other ⁻OH species. This can be rationalized by the μ-bridging ⁻OH groups in this compound having less electron density to contribute to each Tc center than a monodentate ⁻OH.

284 XPS of $[fac\text{-Tc}(\text{CO})_3]^+$ complexes

285 X-ray photoelectron spectroscopy (XPS) is a powerful tool to probe Tc oxidation states; however, its
 286 application is hindered by the extremely limited database and lack of adequate XPS data for low-valent
 287 Tc. For instance, the NIST XPS database contains only 20 entries for Tc.¹⁷ XPS spectra of only two Tc(I)
 288 complexes, including trimethylphosphite and dimethylmethylphosphonite, have been reported.²⁶ Further,
 289 the authors reported that the formal oxidation state of Tc(I) in these complexes was estimated by the
 290 extrapolation of the XPS binding energies of the Tc(IV) and Tc(VII) compounds and was not verified by
 291 an independent method. To date, $[fac\text{-Tc}(\text{CO})_3]^+$ complexes have not been characterized by XPS. The
 292 XPS spectra collected in this study are shown in Figure 4 and the observed Tc binding energy values are
 293 given in Table 3. All $[fac\text{-Tc}(\text{CO})_3]^+$ complexes exhibited characteristic pairs of Tc $3d_{5/2}/3d_{3/2}$ spectral
 294 bands separated by 3.6 eV. For clarity, only Tc $3d_{5/2}$ spectral profiles are considered in the following
 295 discussion. The corresponding electron binding energy for the $[fac\text{-Tc}(\text{CO})_3]^+$ complexes varied from
 296 254.2 eV for $[fac\text{-Tc}(\text{CO})_3\text{Cl}_3]^{2-}$ to 255.4 eV for $[fac\text{-Tc}(\text{CO})_3(\text{OH})_4]$. This provided the opportunity to
 297 systematically evaluate effect of the ancillary ligand coordinated to the $[fac\text{-Tc}(\text{CO})_3]^+$ moiety on the
 298 electronic properties of the Tc(I) center.

299 The XPS spectra of the solid $(\text{Et}_4\text{N})_2[fac\text{-Tc}(\text{CO})_3\text{Cl}_3]$ and $[fac\text{-Tc}(\text{CO})_3(\text{OH})_4]$ compounds showed a
 300 set of doublets, with $3d_{5/2}$ electron binding energies of the dominant form at 254.2 eV and 255.4 eV,
 301 respectively. The binding energy of $(\text{Et}_4\text{N})_2[fac\text{-Tc}(\text{CO})_3\text{Cl}_3]$ is closer to the two literature-reported Tc(I)
 302 species (253.6 – 253.8 eV), while the binding energies of $[\text{Tc}(\text{CO})_3(\text{OH})_4]$ species are significantly greater
 303 and are closer to that reported for Tc(III) (255.3 – 255.7 eV).¹⁷ This is consistent with the IR spectra,
 304 which showed a higher CO stretching frequency for $[\text{Tc}(\text{CO})_3(\text{OH})_4]$ than for $(\text{Et}_4\text{N})_2[fac\text{-Tc}(\text{CO})_3\text{Cl}_3]$.
 305 While such a shift is not completely unexpected based on the changes in the electronic environment
 306 around the $[fac\text{-Tc}(\text{CO})_3]^+$ center caused by the changes in the ancillary ligands, it highlights the need for
 307 creating an XPS spectral library with a diverse range of Tc electronic structures that can demonstrate the
 308 effect of ligand binding on the electronic structure and the oxidation states. Fitting of the spectrum of
 309 $(\text{Et}_4\text{N})_2[fac\text{-Tc}(\text{CO})_3\text{Cl}_3]$ suggests that in addition to Tc(I) it contains three minor components with the
 310 $3d_{5/2}$ electron binding energy positioned at 255.5 eV, 256.8 eV and another at 258.4. The binding energy
 311 of 255.5 eV is similar to that of a $\text{K}_2\text{Tc}_2\text{Cl}_6 \cdot 2\text{H}_2\text{O}$ species with bridging chlorides reported by Gerasimov
 312 *et al.*¹⁶ The assignment of the oxidation state of the previously reported species remains ambiguous,
 313 warranting further studies. The binding energy of 256.8 eV can be tentatively assigned to at Tc(IV)
 314 species arising out of the TcCl_6^{2-} side product, its binding energy is slightly lower than that reported in the
 315 literature. Similarly, the peak with binding energy of 258.4 eV is assigned to presumably arise from a
 316 Tc(V) species either from the TcOCl_4^- starting material,^{27,28} or from a related congener species
 317 (representative example being TcOCl_5^{2-}).¹⁶ Similarly, small Tc(IV) and Tc(VII) components are observed
 318 for $[fac\text{-Tc}(\text{CO})_3(\text{OH}_2)_2(\text{OH})]$

319 While the binding energy of $(\text{Et}_4\text{N})_2[fac\text{-Tc}(\text{CO})_3\text{Cl}_3]$ being lower than any of the $[fac\text{-}$
 320 $\text{Tc}(\text{CO})_3(\text{OH}_2)_{3-n}(\text{OH})_n]^{1-n}$ may initially appear to contradict the FTIR results, which showed $[fac\text{-}$
 321 $\text{Tc}(\text{CO})_3(\text{OH}_2)_3]^+$ to have the highest carbonyl stretching frequency, the differences can be explained by
 322 the different nature and electron withdrawing character of the Cl^- versus OH^- and OH_2 ligands. Cl is less
 323 electronegative than O; consequently, it is a stronger σ -donor and donates more electron density to the
 324 metal center than either ^-OH or OH_2 . The π -donation is more complex. In general, O is a better π -donor
 325 than Cl due to the more contracted nature of the 2p orbitals of O relative to the 3p orbitals of Cl, which
 326 results in greater π -overlap of Tc with O relative to Cl. For this reason, ^-OH is a better π -donor than Cl^- .

Unlike either Cl^- or OH^- , which can both form two π -bonds, H_2O can only form a single π -bond. As a result, the π -donor trend is $\text{HO}^- > \text{Cl}^- > \text{H}_2\text{O}$ as seen in the IR spectra. However, the CO stretching frequencies do not reflect differences in σ -donation among Cl^- , HO^- , and H_2O . XPS on the other hand is directly probing the metal center core electron density, which includes the effects of both σ - and π -bonding, and shows that the compounds with the more electronegative OH^- and OH_2 ligands are more electron deficient than those with Cl^- .

This binding energy trend is continued for additional Tc carbonyl hydrolysis products of the form $[\text{fac-Tc}(\text{CO})_3(\text{OH}_2)_{3-n}(\text{OH})_n]^{1-n}$ where the XPS spectra show that the $3d_{5/2}$ binding energies of $[\text{fac-Tc}(\text{CO})_3(\text{OH}_2)_3]^+$, $[\text{fac-Tc}(\text{CO})_3(\text{OH}_2)_2(\text{OH})]$ and $[\text{fac-Tc}(\text{CO})_3(\text{OH}_2)(\text{OH})_2]^-$ are 255.2, 255.0 and 254.8 eV respectively. These binding energies are consistent with anionic OH^- having a greater σ -donating effect than the neutral OH_2 , and therefore resulting in a greater electron density on the metal center. This matches the results obtained with IR spectroscopy for the carbonyl stretching frequency which shows an increase in π -backbonding between the Tc and carbonyls as the H_2O ligands are replaced with OH^- .

H_2O and OH^- ligated complexes are observed to have significantly higher binding energies than Cl^- ligated species $[\text{fac-Tc}(\text{CO})_3\text{Cl}_3]^{2-}$. This is attributed to the different nature and electron withdrawing character of the Cl^- vs. O binding groups. Cl^- is less electronegative and a better σ -donor, which results in a lower binding energy. A similar effect of higher binding energies of H_2O ligated complexes compared to the Cl^- analogs is also observed for other transition metals, although such examples are comparatively rare due to scarcity of experimental data. As a representative example, the binding energy of $3d_{5/2}$ line for $[\text{Rh}(\text{NH}_3)_5(\text{OH}_2)]^{3+}$ at 310.8 eV¹⁴ is higher compared to that for $[\text{Rh}(\text{NH}_3)_5\text{Cl}]^{2+}$ at 310.2 eV.²⁹

Among the various $[\text{fac-Tc}(\text{CO})_3(\text{OH}_2)_{3-n}(\text{OH})_n]^{1-n}$ species, the binding energy decreases as the number of OH^- ligands increases. These binding energies are consistent with anionic OH^- having a greater σ -donating effect than the neutral H_2O , and therefore resulting in greater electron density on the metal center. The tetrameric $[\text{fac-Tc}(\text{CO})_3(\text{OH})_4]$ species has the highest binding energy. This is initially counterintuitive as the OH^- ligand is generally more electron donating than H_2O . However, in this instance the triply-bridging $\mu_3\text{-OH}$ ligand forms a single σ -bond to each of three different $[\text{fac-Tc}(\text{CO})_3]^+$ moieties, which leaves no lone pairs to act as formal π -donors. As a result, the $\mu_3\text{-OH}$ is electron deficient relative to H_2O , which can act as both a σ - and π -donor. Comparison of this trend with other elements of group 7 in the periodic table is not possible due to unavailability of photoelectron spectra on analogous $[\text{fac-Mn}(\text{CO})_3]^+$ and $[\text{fac-Re}(\text{CO})_3]^+$ complexes (as observed in the NIST XPS database), highlighting the dearth of photoelectron data on these complexes and emphasizing the added importance of such data in evaluating and understanding systematic effects of $\text{OH}^-/\text{H}_2\text{O}$ groups on the electron environment around the $[\text{fac-M}(\text{CO})_3]^+$ framework (M = transition metals belonging to Group 7). To our knowledge, this is the first evaluation of the systematic effects of aqua- versus hydroxo- ligands on the electron density around low-valent $[\text{fac-TM}(\text{CO})_3]^+$ species (TM = any transition metals). Understanding this behavior has implications in many aspects of environmental, biological, and industrial chemistry.

These results demonstrate that the identity of the ancillary ligand has a pronounced impact on the Tc XPS chemical shift in the $[\text{fac-Tc}(\text{CO})_3]^+$ complexes, and results in obscuring its correlation with the metal formal oxidation state evident for the simple inorganic compounds of Tc.¹⁶

XAS

To date, the X-ray Absorption Spectroscopy (XAS) data of the pure Tc(I) complexes belonging to the $[fac\text{-Tc}(\text{CO})_3]^+$ family of aqua ligands are sparse. While XAS studies on $[fac\text{-Tc}(\text{CO})_3]^+$ complexes with chelating ligands such as a bidentate dithioether ligand $[fac\text{-Tc}(\text{CO})_3\text{Cl}(\text{S-S})]$, as well as a tridentate carboxylato thioether or histidine ligand $[fac\text{-Tc}(\text{CO})_3(\text{S-S-O})]$ and $[fac\text{-Tc}(\text{CO})_3]^+\cdot\text{histidine}]$ have been reported,³⁰ a more systematic study is required for complexes with aqua/hydroxo ligands to complement our efforts in NMR, IR and XPS studies to more fully understand how the changing electronic structure of the Tc center with a simple variation of these ligands affects the bond distances. Lukens and coworkers investigated this effect partly in the complexes $[fac\text{-Tc}(\text{CO})_3(\text{OH}_2)_3]^+$, $[fac\text{-Tc}(\text{CO})_3(\text{OH}_2)_2(\text{OH})]$, and $[fac\text{-Tc}(\text{CO})_3(\text{glucoconate})]$.¹⁰ Our efforts here are directed towards consolidating their reference database with the data for $[fac\text{-Tc}(\text{CO})_3\text{Cl}_3]^{2-}$ and $[fac\text{-Tc}(\text{CO})_3(\text{OH})_4]$. Meaningful Tc(I) data for $[fac\text{-Tc}(\text{CO})_3(\text{OH}_2)(\text{OH})_2]^-$ were not obtainable due to the instability of the species with respect to oxidation to TcO_4^- .

The XAS of the starting $[fac\text{-Tc}(\text{CO})_3\text{Cl}_3]^{2-}$ has not been reported before. The fitting results are given in **Error! Reference source not found.** and shown in **Error! Reference source not found.**. From fit, the Tc-CO distances were observed to be 1.909(7) Å, while the Tc-Cl distances were observed to be 2.511(8) Å. The distances are comparable to similar distances in analogous complexes; as a representative example, in the complex $[fac\text{-TcCl}(\text{CN}^t\text{Bu})_2(\text{CO})_3]$, the *trans*-Cl Tc-CO distance is observed to be 1.914(7) Å, while the corresponding Tc-Cl distance is observed to be 2.496(2) Å.¹⁴ The EXAFS data are consistent with the presence of $[fac\text{-Tc}(\text{CO})_3\text{Cl}_3]^{2-}$, and show no evidence of additional Tc species in other oxidation states in the sample, most notably TcO_4^- , suggesting that the obtained $[\text{Tc}(\text{CO})_3\text{Cl}_3]^{2-}$ data can be used as an appropriate reference standard for future XANES analyses. Likewise, the XAS of $[fac\text{-Tc}(\text{CO})_3(\text{OH})_4]$ has not been previously reported, and the fitting results are given in Table 4 and Figure 5.

Obtaining a similar high resolution XAS spectrum for the aqua $[fac\text{-Tc}(\text{CO})_3]^+$ species represented by $[fac\text{-Tc}(\text{CO})_3(\text{OH})_4]$ and $[fac\text{-Tc}(\text{CO})_3(\text{OH}_2)_{3-n}(\text{OH})_n]^{1-n}$ ($n=0-3$) is challenging due to the inherent tendency of the low oxidation state Tc(I) containing $[fac\text{-Tc}(\text{CO})_3]^+$ species towards oxidative hydrolysis leading to TcO_4^- . While this affects the spectral quality in general, compromising our ability to fit the data for the exact determination of bond distances and angles, the resulting spectra allow for discerning qualitative systematic trends in terms of the Tc(I) coordination environment. The spectra and structural parameters of the $[fac\text{-Tc}(\text{CO})_3]^+$ complexes, are all similar since the main geometric structure differences between these complexes are small differences in the Tc-O and Tc-CO bond distances and angles.¹⁰ In the series of complexes, it is observed that the distances between Tc and CO for $[fac\text{-Tc}(\text{CO})_3(\text{OH})_4]$ $[fac\text{-Tc}(\text{CO})_3(\text{OH}_2)_3]^+$ $[fac\text{-Tc}(\text{CO})_3(\text{OH}_2)_2(\text{OH})]$ are 1.95(1) Å, 1.905(2) Å, and 1.886(3) Å, respectively, and their C≡O distances are 1.10(2) Å, 1.14(1) Å, and 1.20(1) Å, respectively. The complex with the weakest σ and π -donor ligands is $[fac\text{-Tc}(\text{CO})_3(\text{OH})_4]$ because OH^- groups are μ_3 -bridging and consequently unable to π -donate, compared to terminal OH^- or OH_2 groups. The $[fac\text{-Tc}(\text{CO})_3(\text{OH}_2)_3]^+$ complex comes next, having slightly shorter Tc-O and slightly longer C≡O distance, consistent with that reported by Lukens *et al.*¹⁰ Substitution of a single water ligand by a hydroxide group in $[fac\text{-Tc}(\text{CO})_3(\text{HO})(\text{OH}_2)_2]$ results in reducing the average Tc-O distance while simultaneously increasing the CO distance due to hydroxide being a stronger σ and π -donor ligand than water. This result is consistent with that observed by Lukens *et al.*¹⁰

Conclusions

The $[fac\text{-Tc}(\text{CO})_3\text{L}_3]^+$ moiety is of fundamental importance to both nuclear medicine and the remediation of nuclear wastes. Despite this fact, many compounds within this class are not fully characterized with respect to their spectroscopic signatures or electronic structure. Characterization of Tc compounds in the less common oxidation states can be a challenge because of the sparse spectroscopic data in the scientific literature. In order to more firmly establish a “spectroscopic library” of Tc compounds in the scientific literature, $[fac\text{-Tc}(\text{CO})_3\text{Cl}_3]^{2-}$, and compounds of the general formula $[fac\text{-Tc}(\text{CO})_3(\text{OH}_2)_{3-n}(\text{OH})_n]^{1-n}$ have been characterized by NMR, IR, XPS and XAS. The IR spectroscopy shows a gradual decrease in carbonyl stretching frequency with increasing OH substitution as a consequence of increased metal center electron density for $[fac\text{-Tc}(\text{CO})_3(\text{OH}_2)_{3-n}(\text{OH})_n]^{1-n}$ molecules. XPS confirms interpretation of the IR spectroscopy, providing a systematic evaluation of the metal center core electron density, and to our knowledge is the first XPS data collected for group 7 $[fac\text{-M}(\text{CO})_3(\text{OH}_2)_{3-n}(\text{OH})_n]^{1-n}$ compounds. The present study also reports the first example of XAS data for $[fac\text{-Tc}(\text{CO})_3\text{Cl}_3]^{2-}$. The obtained structural parameters agree within experimental error of what would be anticipated from the crystal structures of similar literature compounds.

Acknowledgements

This research was supported by the U.S. Department of Energy’s Office of Environmental Management and performed as part of the Technetium Management Hanford Site project at the Pacific Northwest National Laboratory (PNNL) operated by Battelle for the U.S. Department of Energy under Contract DE-AC05-76RL01830. Part of this research was performed at EMSL, a national scientific user facility at PNNL managed by the Department of Energy’s Office of Biological and Environmental Research. Tc K-edge XAFS spectra were obtained at the Advanced Photon Source, a national scientific user facility at Argonne National Laboratory managed by the Department of Energy’s Office of Science, and at the Stanford Synchrotron Radiation Lightsource, SLAC National Accelerator Laboratory, which is supported by the U.S. Department of Energy, Office of Science, Office of Basic Energy Sciences under Contract No. DE-AC02-76SF00515. XAFS analysis was supported by the U.S. Department of Energy, Office of Science, Basic Energy Sciences, Chemical Sciences, Biosciences, and Geosciences Division, Heavy Element Chemistry Program and was performed at Lawrence Berkeley National Laboratory under contract No. DE-AC02-05CH11231. The authors would like to especially acknowledge Dr. Nicholas Machara for the stewardship of this research.

References

- (1) Fischer, E. O.; Jira, R. *Zeitschrift fuer Naturforsch.* **1954**, *9b*, 618–619.
- (2) Alberto, R.; Schibli, R.; Waibel, R.; Abram, U.; Schubiger, A. P. *Coord. Chem. Rev.* **1999**, *190–192*, 901–919.
- (3) Sulieman, S.; Can, D.; Mertens, J.; N'Dongo, H. W. P.; Liu, Y.; Schmutz, P.; Bauwens, M.; Spingler, B.; Alberto, R. *Organometallics* **2012**, *31* (19), 6880–6886.
- (4) Brink, A.; Visser, H. G.; Roodt, A. *Inorg. Chem.* **2014**, *53* (23), 12480–12488.
- (5) Schulte, E. H.; Scoppa, P. *Sci. Total Environ.* **1987**, *64* (1–2), 163–179.
- (6) Wildung, R.; McFadden, K.; Garland, T. *J. Environ. Qual.* **1979**, *8*, 156–161.
- (7) Schroeder, N.; Radzinski, S.; Ashley, K.; Truong, A.; Sczcepaniak, P. In *Science and Technology for Disposal of Radioactive Tank Wastes*; Schulz, W., Lombardo, N., Eds.; Plenum Press: New York, USA, 1998; pp 301–320.
- (8) Golcar, G.; NG Colton, N.; Darab, J.; Smith, H. *Hanford Waste Tank Simulants Specification and Their Applicability for the Retrieval, Pretreatment, and Vitrification Processes*; Richland, WA, 2000.
- (9) Schroeder, N. C.; Radzinski, S. D.; Ashley, K. R.; Truong, A. P.; Whitener, G. D. *J. Radioanal. Nucl. Chem.* **2001**, *250* (2), 271–284.
- (10) Lukens, W. W.; Shuh, D. K.; Schroeder, N. C.; Ashley, K. R. *Environ. Sci. Technol.* **2004**, *38* (1), 229–233.
- (11) Schroeder, N. C.; Ashley, K. R. *J. Radioanal. Nucl. Chem.* **2005**, *263* (3), 567–573.
- (12) Alberto, R. In *Medicinal Organometallic chemistry*; Metzler-Nolte, J., Ed.; Springer Berlin Heidelberg, 2010; pp 221–246.
- (13) Gorshkov N.I., Lumpov, A.A. Miroslavov, A.E. Suglobov, D. N. *Radiochemistry* **2000**, *45* (2), 116–119.
- (14) Alberto, R.; Schibli, R.; Egli, A.; August Schubiger, P.; Herrmann, W. a.; Artus, G.; Abram, U.; Kaden, T. a. *J. Organomet. Chem.* **1995**, *493* (1–2), 119–127.
- (15) Helm, L. *Coord. Chem. Rev.* **2008**, *252* (21–22), 2346–2361.
- (16) Gerasimov, V. N.; Kryuchkov, S. V.; Kuzina, A. F.; Kulakov, V. M.; Pirozhkov, S. V.; Spitsyn, V. I. *Doki. Akad. Nauk. SSSR, Engl. Transl.* **1982**, *266*, 148.
- (17) Naumkin, A. V.; Kraut-Vass, A.; Gaarenstroom, S. W.; Powell, C. J. In *NIST Standard Reference Database 20, Version 4.1*; National Institute of Standards and Technology: Gaithersburg, MD, 2012.

- 468 (18) Hall, G. B.; Chatterjee, S.; Levitskaia, T. G.; Martin, T.; Wall, N.; Walter, E. D. *Synthesis*
469 *and Characterization of Tc(I) Carbonyl Nitrosyl Species Relevant to the Hanford Tank Waste: FY 2016*
470 *Status Report*; Richland, WA, 2015.
- 471 (19) Alberto, R.; Schibli, R.; Egli, A.; Abram, U.; Abram, S.; Kaden, T. A.; August Schubiger, P.
472 *Polyhedron* **1998**, 17 (7), 1133–1140.
- 473 (20) Cho, H.; De Jong, W. A.; McNamara, B. K.; Rapko, B. M.; Burgeson, I. E. *J. Am. Chem. Soc.*
474 **2004**, 126 (37), 11583–11588.
- 475 (21) Franklin, K. J.; Lock, C. J. L.; Sayer, B. G.; Schrobilgen, G. J. *J. Am. Chem. Soc.* **1982**, 104
476 (20), 5303–5306.
- 477 (22) Rehr, J. J.; Albers, R. C.; Zabinsky, S. I. *Phys. Rev. Lett.* **1992**, 69 (23), 3397–3400.
- 478 (23) Lukens, W. W.; Bucher, J. J.; Edelstein, N. M.; Shuh, D. K. *Environ. Sci. Technol.* **2002**, 36
479 (5), 1124–1129.
- 480 (24) Aebischer, N.; Schibli, R.; Alberto, R. *Angew. Chem. Int. Ed.* **2000**, 3 (1), 254–256.
- 481 (25) Grundler, P. V.; Helm, L.; Alberto, R.; Merbach, A. E. *Inorg. Chem.* **2006**, 45 (25), 10378–
482 10390.
- 483 (26) Wester, D. W.; White, D. H.; Miller, F. W.; Dean, R. T.; Schreifels, J. A.; Hunt, J. E.
484 *Inorganica Chim. Acta* **1987**, 131, 163–169.
- 485 (27) Thompson, M.; Nunn, A. D.; Treher, E. N. *Society* **1986**, 3103 (13), 3100–3103.
- 486 (28) Wester, D. W.; White, D. H.; Miller, F. W.; Dean, R. T. *Inorganica Chim. Acta* **1987**, 131,
487 163–169.
- 488 (29) Andersson, S. L. T.; Scurrrell, M. S. *J. Catal.* **1981**, 71 (2), 233–243.
- 489 (30) Seifert, S.; Ku, J. *Inorganica Chim. Acta* **2001**, 322, 79–86.
490

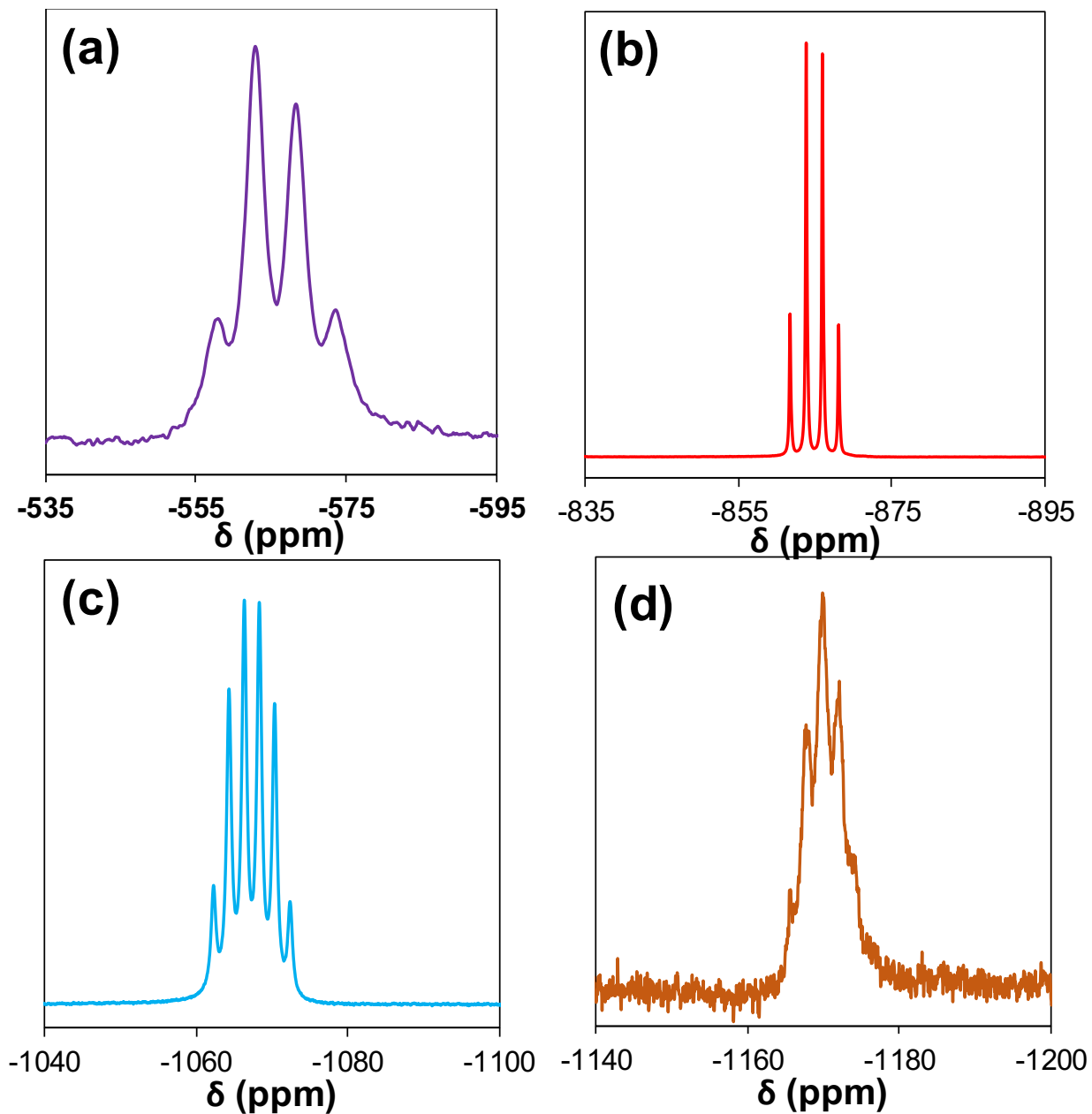


Figure 1. Solution state ^{99}Tc NMR spectrum of the $[\text{Tc}^{(13}\text{CO})_3]^+$ species. (a) $[\text{Tc}^{(13}\text{CO})_3(\text{OH})]_4$ in 5M NaNO_3 at pH = 7 – 11, (b) $[\text{Tc}^{(13}\text{CO})_3(\text{H}_2\text{O})_3]^+$ in 5M NaNO_3 at pH = 1, (c) $[\text{Tc}^{(13}\text{CO})_3(\text{H}_2\text{O})_2(\text{OH})]$ in 5M $\text{NaNO}_3/0.1\text{M}$ NaOH , (d) $[\text{Tc}^{(13}\text{CO})_3(\text{H}_2\text{O})(\text{OH})_2]^-$ in 6.2M NaOH .

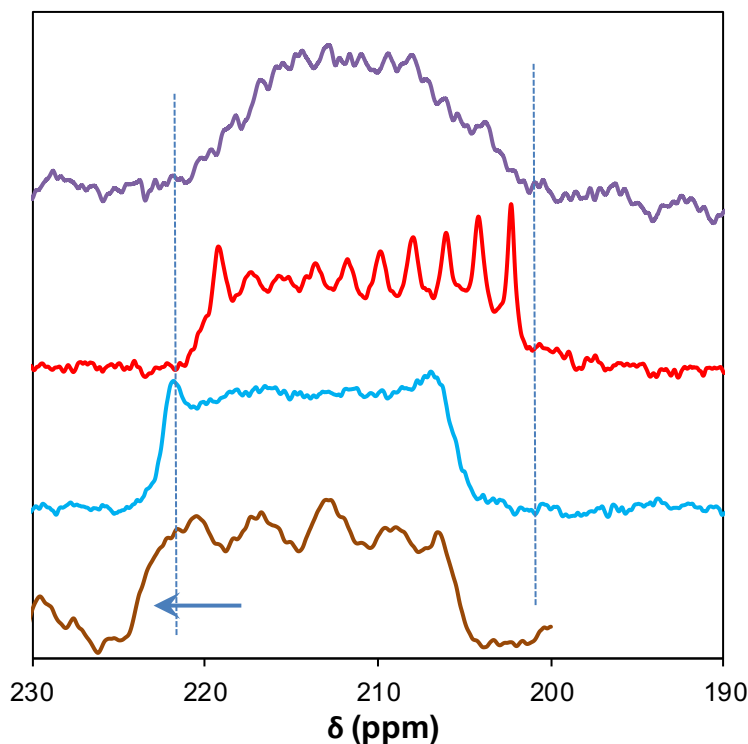


Figure 2. Solution state ^{13}C NMR spectrum of the $[\text{Tc}(^{13}\text{CO})_3]^+$ species in solution. Top, violet trace: $[\text{Tc}(^{13}\text{CO})_3(\text{OH})]_4$ in 5M NaNO_3 at pH = 7 – 11. Second from top, red trace: $[\text{Tc}(^{13}\text{CO})_3(\text{H}_2\text{O})_3]^+$ in 5M NaNO_3 at pH = 1. Second from bottom, light blue trace: $[\text{Tc}(^{13}\text{CO})_3(\text{H}_2\text{O})_2(\text{OH})]$ in 5M $\text{NaNO}_3/0.1\text{M}$ NaOH . Bottom, brown trace: $[\text{Tc}(^{13}\text{CO})_3(\text{H}_2\text{O})(\text{OH})_2]^-$ in 6.2M NaOH .

Table 1. Tabulation of the NMR chemical shifts and coupling constants for the $[\text{Tc}(\text{CO})_3]^+$ compounds.

Complex	Solvent medium	Chemical shift (cm^{-1})		$^1J_{99\text{Tc},^{13}\text{C}}$
		Unlabelled	Labelled	
$[\text{fac-Tc}(\text{CO})_3(\text{OH})]_4$	H_2O with appropriate supporting electrolyte	-583	-568	418
$[\text{fac-Tc}(\text{CO})_3(\text{H}_2\text{O})_3]^+$		-869	-865	395
$[\text{fac-Tc}(\text{CO})_3(\text{H}_2\text{O})_2(\text{OH})]$		-1069	-1067	385
$[\text{fac-Tc}(\text{CO})_3(\text{H}_2\text{O})(\text{OH})_2]^-$		-1146	-1168	403

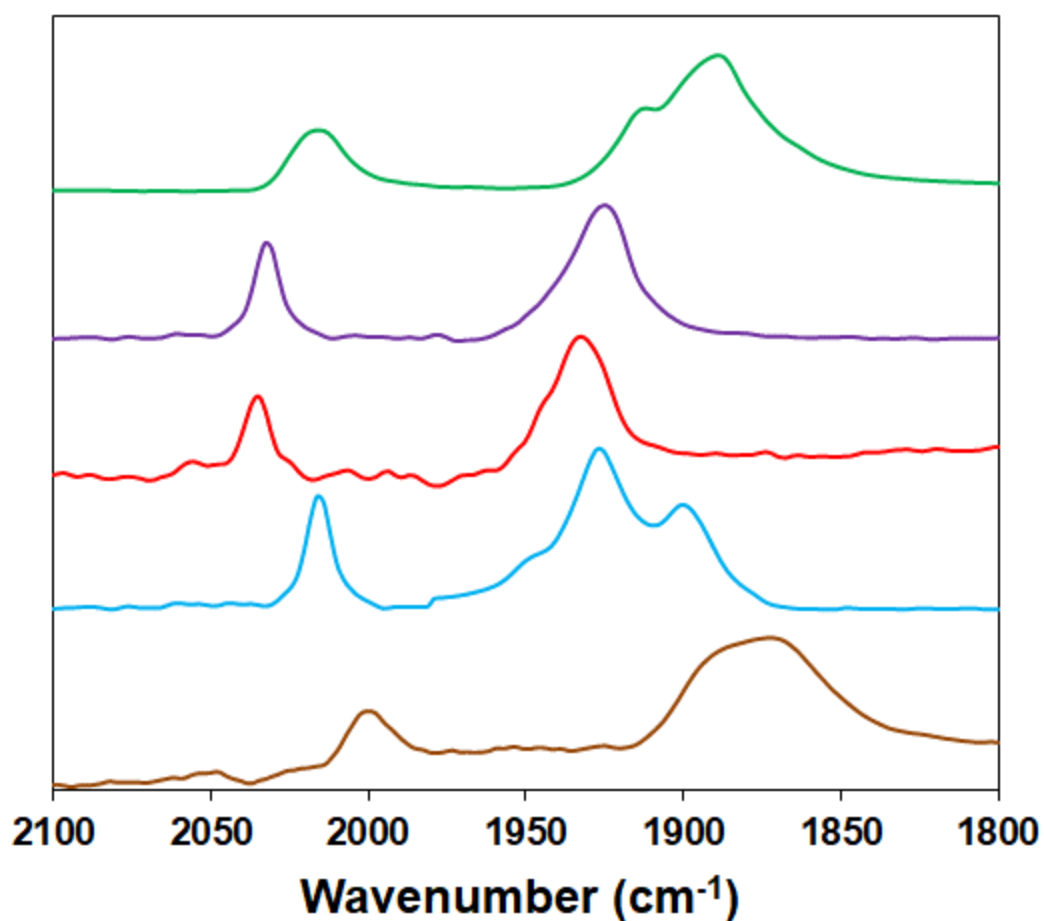


Figure 3. Carbonyl IR spectral region of the $[\text{Tc}(\text{CO})_3]^+$ species. Top, green trace: solid $[\text{Tc}(\text{CO})_3\text{Cl}_3]^{2-}$ powder. Second from top, violet trace: $[\text{Tc}(\text{CO})_3(\text{OH})_4]$ in 5M NaNO_3 at pH = 7 – 11. Middle, red trace: $[\text{Tc}(\text{CO})_3(\text{H}_2\text{O})_3]^+$ in 5M NaNO_3 at pH = 1. Second from bottom, light blue trace: $[\text{Tc}(\text{CO})_3(\text{H}_2\text{O})_2(\text{OH})]$ in 5M $\text{NaNO}_3/0.1\text{M NaOH}$. Bottom, brown trace: $[\text{Tc}(\text{CO})_3(\text{H}_2\text{O})(\text{OH})_2]^-$ in 6.2M NaOH .

Table 2. Tabulation of the IR vibrations of the $[\text{Tc}(\text{CO})_3]^+$ compounds in in the Tc-CO region.

Complex	CO vibrations (cm^{-1})
$[\text{Tc}(\text{CO})_3(\text{H}_2\text{O})_3]^+$	1931, 1943(sh), 2036
$[\text{Tc}(\text{CO})_3(\text{OH})_4]$	1925, 1939(sh), 2032
$[\text{Tc}(\text{CO})_3(\text{H}_2\text{O})_2(\text{OH})]$	1898, 1923, 1945(sh), 2016
$[\text{Tc}(\text{CO})_3(\text{H}_2\text{O})(\text{OH})_2]^-$	1870, 1890, 2000

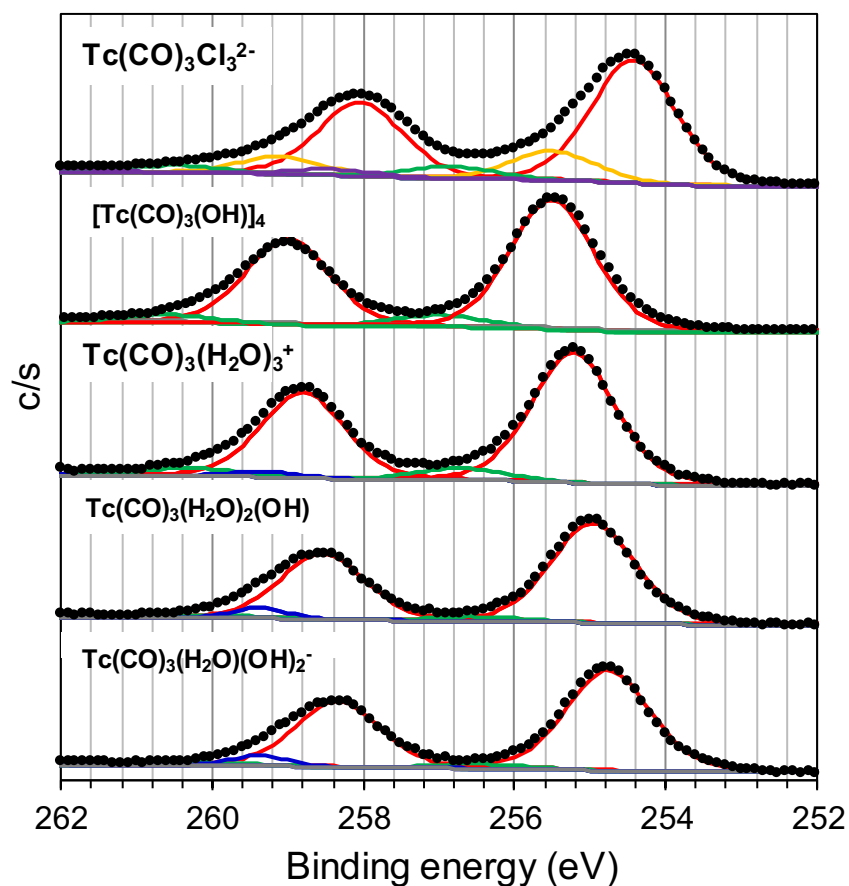


Figure 4. X-ray photoelectron spectra of Tc $3d_{5/2}$ and $3d_{3/2}$ regions for $(\text{Et}_4\text{N})_2[\text{Tc}(\text{CO})_3\text{Cl}_3]$, $[\text{Tc}(\text{CO})_3(\text{OH})]_4$, $[\text{Tc}(\text{CO})_3(\text{H}_2\text{O})_3]^+$, $[\text{Tc}(\text{CO})_3(\text{H}_2\text{O})_2(\text{OH})]$ and $[\text{Tc}(\text{CO})_3(\text{H}_2\text{O})(\text{OH})_2]^-$. Black circles = experimental spectrum, red trace = Tc(I) fit, green trace = Tc(IV) fit based on literature, violet trace = Tc(V) based on literature, blue trace = Tc(VII) fit based on literature.

Table 3. Tc $3d_{5/2}$ binding energies of $[\text{fac-Tc}(\text{CO})_3(\text{H}_2\text{O})_{3-n}(\text{OH})_n]^{1-n}$ compounds as determined by XPS.

Compound	Tc $3d_{5/2}$ electron binding energy (eV)
$[\text{Tc}(\text{CO})_3(\text{OH})]_4$	255.4
$[\text{Tc}(\text{CO})_3(\text{H}_2\text{O})_3]^+$	255.2
$[\text{Tc}(\text{CO})_3(\text{H}_2\text{O})_2(\text{OH})]$	255.0
$[\text{Tc}(\text{CO})_3(\text{H}_2\text{O})(\text{OH})_2]^-$	254.8
$(\text{Et}_4\text{N})_2[\text{Tc}(\text{CO})_3\text{Cl}_3]^{2-}$	254.2

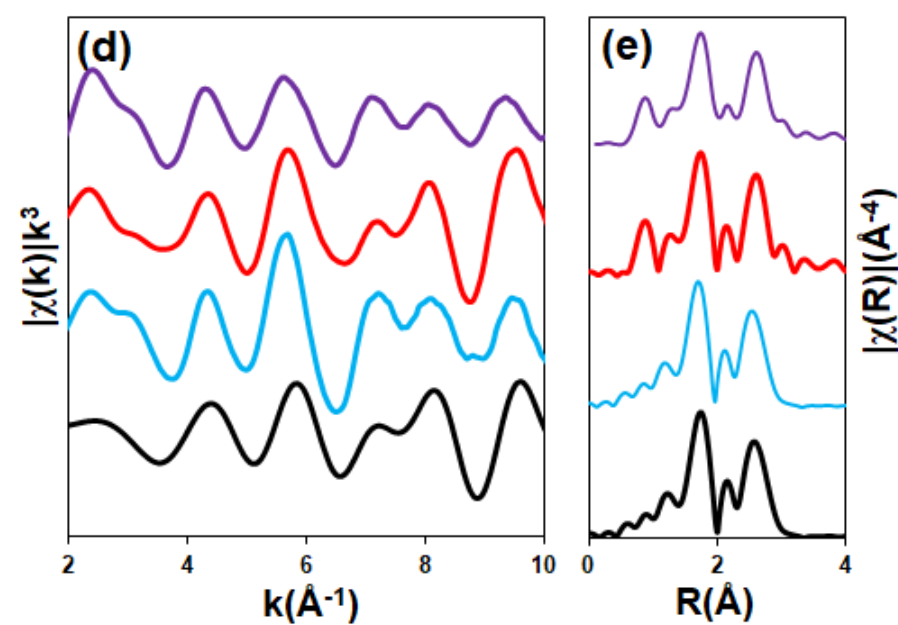
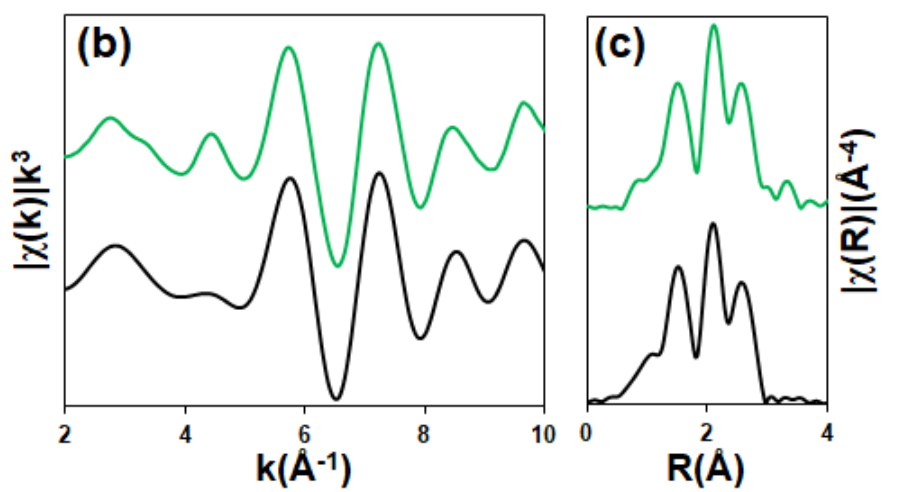
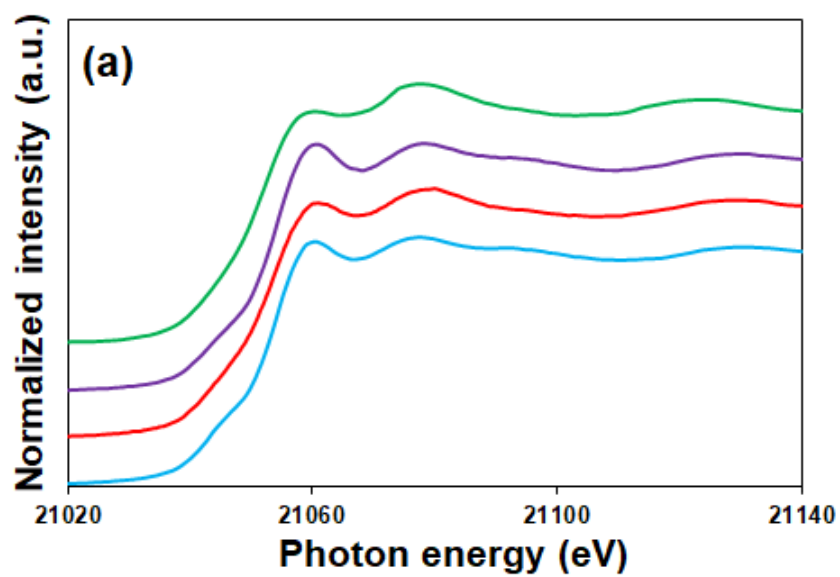


Figure 5. (a) EXAFS spectra of various $[fac\text{-Tc}(\text{CO})_3]^+$ species in energy space. Top, green trace: $(\text{Et}_4\text{N})_2[\text{Tc}(\text{CO})_3\text{Cl}_3]$ solid. Second from top, violet trace: $[\text{Tc}(\text{CO})_3(\text{OH})]_4$. Second from bottom, red trace: $[\text{Tc}(\text{CO})_3(\text{H}_2\text{O})_3]^+$. Bottom light blue trace: $[\text{Tc}(\text{CO})_3(\text{H}_2\text{O})_2(\text{OH})]$. (b) EXAFS spectra of $(\text{Et}_4\text{N})_2[\text{Tc}(\text{CO})_3\text{Cl}_3]$ in k-space and (c) the corresponding Fourier transforms. Top, green trace: $(\text{Et}_4\text{N})_2[\text{Tc}(\text{CO})_3\text{Cl}_3]$ solid from this work. Bottom, black trace: literature data.(reference). (d) EXAFS spectra of $[fac\text{-Tc}(\text{CO})_3(\text{H}_2\text{O})_{3-n}(\text{OH})_n]^{1-n}$ ($n=0\text{-}2$) in k-space and (e) the corresponding Fourier transforms. Top, violet trace: $[\text{Tc}(\text{CO})_3(\text{OH})]_4$. Second from top, red trace: $[\text{Tc}(\text{CO})_3(\text{H}_2\text{O})_3]^+$. Second from bottom light blue trace: $[\text{Tc}(\text{CO})_3(\text{H}_2\text{O})_2(\text{OH})]$. Bottom, black trace: literature fit.

Table 4. EXAFS fit parameters.

$(\text{Et}_4\text{N})_2[\text{Tc}(\text{CO})_3\text{Cl}_3]^a$					
Neighbor	# of Neighbors ^b	Distance (Å)	σ^2 (Å ²)	π	
C	3	1.909(7)	0.0026(6)	<0.001	
Cl	3	2.511(8)	0.0038(5)	<0.001	
O	3	3.21(2)	0.0015(7)	0.006	
O-C-Tc-C-O (MS)	3	2.991(9)	0.0015(7) ^c	<0.001	
$[\text{Tc}(\text{CO})_3(\text{H}_2\text{O})_3]^{+,d}$					
Neighbor	# of Neighbors	Distance (Å)	σ^2 (Å ²)	π	Distance From EST 2004
C	2.3(3)	1.95(1)	0.0016(6) ^e	0.001	1.904(2)
O	2.3(3)	2.173(7)	0.0021(8) ^e	<0.001	2.163(2)
Tc	0.3(3)	2.85(2)	0.0016(6) ^e	0.033	3.96(1)
O ^f	2.3(3)	3.054(8)	0.0016(6) ^e	<0.001	3.045(9)
C	0.9(1)	3.63(4)	0.0016(6) ^e	0.024	--
Trans-MS	4.6(6)	4.00(1)	0.003(1) ^e	0.014	3.96(2)

- a) $S_0^2=1$ (fixed), $\Delta E=0(2)$ eV; fit range $2 < k < 14$; $1.1 < R < 3$; # of independent points: 16.2; # of parameters: 8, r_factor 0.016; standard deviations are given in parentheses and are in the same units as the last digit.
- b) Parameter fixed
- c) Parameter constrained to equal that of the previous shell.
- d) $S_0^2=0.9$ (fixed), $\Delta E= 10(1)$
- e) Parameter is constrained by that of the TcO_4^- shell.

- f) This path includes two multiple scattering path to the carbonyl oxygen atom.